4-15-2011

First-principles analysis of ZrN/ScN metal/semiconductor superlattices for thermoelectric energy conversion

Bivas Saha
Birck Nanotechnology Center, Purdue University, bsaha@purdue.edu

Timothy D. Sands
Birck Nanotechnology Center, Purdue University, tsands@purdue.edu

Umesh V. Waghmare
Jawaharlal Nehru Center for Advanced Scientific Research

AIP | Journal of Applied Physics

First-principles analysis of ZrN/ScN metal/semiconductor superlattices for thermoelectric energy conversion

Bivas Saha, Timothy D. Sands, and Umesh V. Waghmare

Citation: J. Appl. Phys. **109**, 083717 (2011); doi: 10.1063/1.3569734
View online: http://dx.doi.org/10.1063/1.3569734
View Table of Contents: http://jap.aip.org/resource/1/JAPIAU/v109/i8
Published by the AIP Publishing LLC.

First-principles analysis of ZrN/ScN metal/semiconductor superlattices for thermoelectric energy conversion

Bivas Saha,[1,a)] Timothy D. Sands,[1,2] and Umesh V. Waghmare[3]
[1]*School of Materials Engineering and Birck Nanotechnology Center, Purdue University, West Lafayette, Indiana 49707, USA*
[2]*School of Electrical and Computer Engineering, Purdue University, West Lafayette, Indiana 49707, USA*
[3]*Theoretical Sciences Unit, Jawaharlal Nehru Centre for Advanced Scientific Research, Jakkur, Bangalore 560064, India*

(Received 9 October 2010; accepted 19 February 2011; published online 22 April 2011)

We present a first-principles density functional theory-based analysis of the electronic structure, vibrational spectra, and transport properties of ZrN/ScN metal/semiconductor superlattices aiming to understand its potential and suitability for thermoelectric applications. We demonstrate (a) the presence of Schottky barriers of 0.34 eV at the metal/semiconductor interface and (b) a large asymmetry in the electronic densities of states and flattening of electronic bands along the cross-plane directions near the Fermi energy of these superlattices, desirable for high Seebeck coefficient. The vibrational spectra of these superlattices show softening of transverse acoustic phonon modes along the growth direction and localization of ScN phonons in the vibrational energy gap between metal and semiconductor layers. Boltzmann transport theory-based analysis suggests a reduction of lattice thermal conductivity by an order of magnitude compared to its individual bulk components, which makes these materials suitable for thermoelectric applications. [doi:10.1063/1.3569734]

I. INTRODUCTION

Thermoelectric materials that convert heat flux directly into electrical power have enormous promise in dealing with the challenges of the growing demand for alternative clean energy, and are a subject of great scientific interest.[1,2] These materials are characterized by a dimensionless figure of merit $ZT = S^2\sigma T/\kappa$, where S is the Seebeck coefficient, σ is the electrical conductivity, κ is the thermal conductivity, and T is the absolute temperature. To be competitive with conventional refrigerators and power generators, we must develop materials with $ZT = 3$–4. Research in the last few years with conventional bulk materials[3,4] has yielded ZT of about 1.0–1.5. Achieving $ZT > 2$ is challenging due to mutually conflicting design parameters (e.g., σ and κ) in ZT. Pioneering works of Hicks and Dresselhaus[5,6] and subsequent experiments of Harman *et al.*[7] and Venkatasubramanian *et al.*[8] showed that nanostructured materials have the potential for higher ZT.

Multilayers and superlattices[9–11] grown by alternate deposition of metal and semiconductor materials with nanoscale periods are being explored as potential candidates with higher ZT. The central ideas are (1) to control the Schottky barrier height for efficient energy filtering of electrons during transport, thereby enhancing the Seebeck coefficient, simultaneously retaining a high electrical conductivity, and (2) to use the interface between the component materials as a phonon filter, thereby reducing the cross-plane lattice thermal conductivity. Understanding the nature of the metal/semiconductor interface is crucial to designing multilayers or superlattices with high ZT.

In this paper, we present first-principles density functional theory-based calculations of electronic structure and vibrational spectra, as a foundation for developing an understanding of the temperature-dependent cross-plane transport properties of ZrN/ScN metal/semiconductor superlattices. We note that ScN is semiconducting in nature with an indirect Γ–X bandgap of 0.89 eV, whereas ZrN is metallic in nature.[12] Their multilayers (superlattices) have been investigated experimentally in earlier work by Rawat *et al.*[13]

II. METHODS OF CALCULATIONS

We use the PWSCF implementation of the density functional theory with a generalized gradient approximation (GGA)[14] to the exchange correlation energy and ultrasoft pseudopotentials[15] to represent the interaction between ionic cores and valence electrons. Plane wave basis sets with energy cutoffs of 30 and 180 Ry were used to represent the electronic wave function and charge density, respectively. Integration over the Brillouin zone is carried out using the Monkhorst–Pack[16] scheme with a $10 \times 10 \times 10/n$ mesh of k-points for n/n superlattice, and occupation numbers are smeared using the Methfessel–Paxton[17] scheme with a broadening of 0.003 Ry. A Hubbard U correction,[18] with $U = 3.5$ eV is included along with GGA for Sc atoms to correctly describe the electronic bandwidth and gap. (See details and validity of our methods used in extensive analysis of bulk properties of ScN, ZrN, and HfN in Ref. 12.)

Phonon spectra and density of states are determined accurately within the framework of self-consistent density functional perturbation theory,[19] with plane wave basis of energy cutoffs of 40 and 750 Ry to describe the wave function and charge density, respectively. In order to understand the detailed features of phonon spectra, force constant matrices were obtained on a $3 \times 3 \times 1$ (for 2/2 superlattice)

[a)]Electronic mail: bsaha@purdue.edu.

q-point mesh. The dynamical matrices at arbitrary wave vectors were then obtained through Fourier transform-based interpolation.

Electrical conductivity (σ) and Seebeck coefficient (S) are calculated within the Boltzmann transport theory

$$\sigma_{\alpha\beta} = e^2 \int_{-\infty}^{\infty} \sum_k v_\alpha(k) v_\beta(k) \tau(k) \delta[\varepsilon - \varepsilon(k)] \left(-\frac{\delta f_0}{\delta \in}\right) d \in,$$

$$S = \frac{e}{T\sigma} \int_{-\infty}^{\infty} \sum_k v_\alpha(k) v_\beta(k) \tau(k) \delta[\varepsilon - \varepsilon(k)](\varepsilon - \mu) \left(-\frac{\delta f_0}{\delta \in}\right) d \in,$$

where $v_\alpha(k)$ and $v_\beta(k)$ are the group velocities of electron in the α and β directions, respectively, $\delta[\varepsilon - \varepsilon(k)]$ is the density of electronic states, $\tau(k)$ is the relaxation time, μ is the chemical potential, and f_0 is the Fermi–Dirac distribution function. Eigenenergies of electrons are calculated on a very dense mesh of k-points in the entire Brillouin zone, and subsequently used to estimate the group velocities.

It is not simple to estimate the electronic relaxation time from first-principles, and hence we do not have the knowledge of $\tau(k)$ for the bulk materials (ZrN, ScN), as well as ZrN/ScN superlattices. Here we assume the electronic relaxation time to be independent of electron energy and about the same for all the materials, and compare their electrical conductivity and Seebeck coefficient. This is an oversimplification, but could give us a trend in electronic contributions to transport properties of these superlattices.

The lattice thermal conductivity $\kappa_{\alpha\beta}$ (i.e., along the $\alpha\beta$ direction) is obtained within the Boltzmann theory

$$\kappa_{\alpha\beta} = \hbar \sum_\lambda \int \frac{d^3q}{(2\pi)^3} v_{\alpha\lambda}(q) v_{\beta\lambda}(q) \omega_\lambda(q) \tau_\lambda(q) \left\{\frac{dn_B[\omega_\lambda(q)]}{dT}\right\},$$

where λ is the polarization vector of the normal mode, $v_{\alpha\lambda}(q)$ and $v_{\beta\lambda}(q)$ are the group velocities of the phonon along α and β directions, respectively, $\tau_\lambda(q)$ is the relaxation time, and $n_B[\omega_\lambda(q)]$ is the Bose–Einstein distribution function. The relaxation time $\tau_\lambda(q)$ is assumed to be constant and kept outside the integral. Eigenfrequencies were obtained on a dense mesh of 1000 k-points over the entire Brillouin zone, which were subsequently used in determination of $v_{\alpha\lambda}(q)$ and $v_{\beta\lambda}(q)$.

III. RESULTS

A. Structural details

ZrN(m)/ScN(n) superlattices were made by periodically stacking m layers of metal and n layers of semiconductor. The in-plane and cross-plane lattice constants are fully optimized and the structures are fully relaxed until forces on each atom are less than 0.001 Ry/bohr. Despite a 1.5% lattice mismatch between the component materials ZrN ($a = 4.59$ Å) and ScN ($a = 4.52$ Å), all superlattices grow epitaxially with an in-plane lattice constant of 4.55 Å, with no significant structural changes in the in-plane direction. Along the cross-plane (growth) direction, different atoms move significantly by different amounts due to the lattice mismatch.

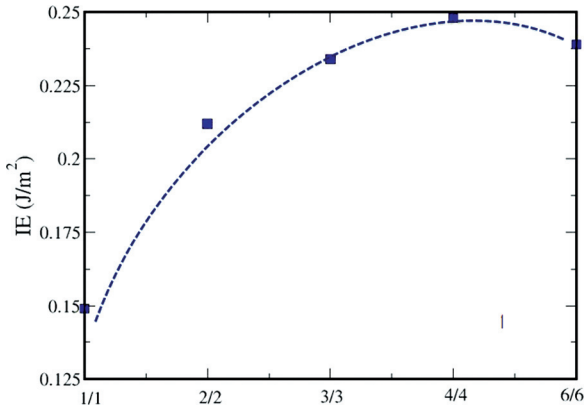

FIG. 1. (Color online) Interface energy density (IED) as a function of periodicity of the superlattices, calculated using the formula $[E_{(\text{bulk}-\text{ZrN})} + E_{(\text{bul}-\text{ScN})} - E_{(\text{ZrN/ScN})}]$. Convergence is achieved quickly with the 4/4, 6/6 superlattice. Lines are drawn over the data points to show convergence.

However, the cross-plane lattice constant increases linearly with an increase in m and n.

The interface energy (IE) of a superlattice is calculated using the following formula:

$$\left[mE_{(\text{bulk}-\text{ZrN})} + nE_{(\text{bulk}-\text{ScN})} - (m+n)E_{(\text{ZrN/ScN})}\right]/a^2,$$

where $E_{(\text{ZrN/ScN})}$, $E_{(\text{bulk-ZrN})}$, and $E_{(\text{bulk-ScN})}$ are the energies of the superlattices, bulk ZrN, and bulk ScN, respectively, and a is the area of the interface. The IEs are positive suggesting the relative stability of these metal/semiconductor interfaces. The values also converge rapidly with an increase in the number of metal and semiconductor layers (see Fig. 1).

B. Electronic structure

Although we have determined the electronic structure of m/n ZrN/ScN superlattices with m and $n = 1$–4, here we present results of (m/m) superlattices. The dispersion spectra of the 2/2 superlattice [generic of all other higher periodic superlattices in Fig. 2(a)] shows that the superlattices are metallic for the in-plane transport (i.e., Γ–X), whereas there are relatively flat bands (near the Fermi energy) along the cross-plane direction (i.e., Γ–Z). These nearly flat bands will increase the effective mass of electrons, thereby increasing the Seebeck coefficient along the cross-plane direction. Figure 2(a) also indicates the presence of doubly degenerate valence bands lying 0.2–0.3 eV (0.2 eV exactly for 2/2 superlattices) below the Fermi energy. The electronic band just above the Fermi energy is also at a distance 0.5 eV from the Fermi energy at the Γ point along the Γ–Z directions suggesting that for cross-plane electronic transport the superlattices behave like a degenerate semiconductor. As the theory of thermoelectric metal/semiconductor superlattices[10,20–23] suggests that to maximize the power factor ($S^2\sigma$) one needs degenerate semiconductor or metallic superlattices with tall barrier height, and nonconserved lateral momentum for the thermionic emission process, our superlattices seem suitable for effectively filtering out low energy electrons at the metal/semiconductor interfaces, enhancing the Seebeck coefficient

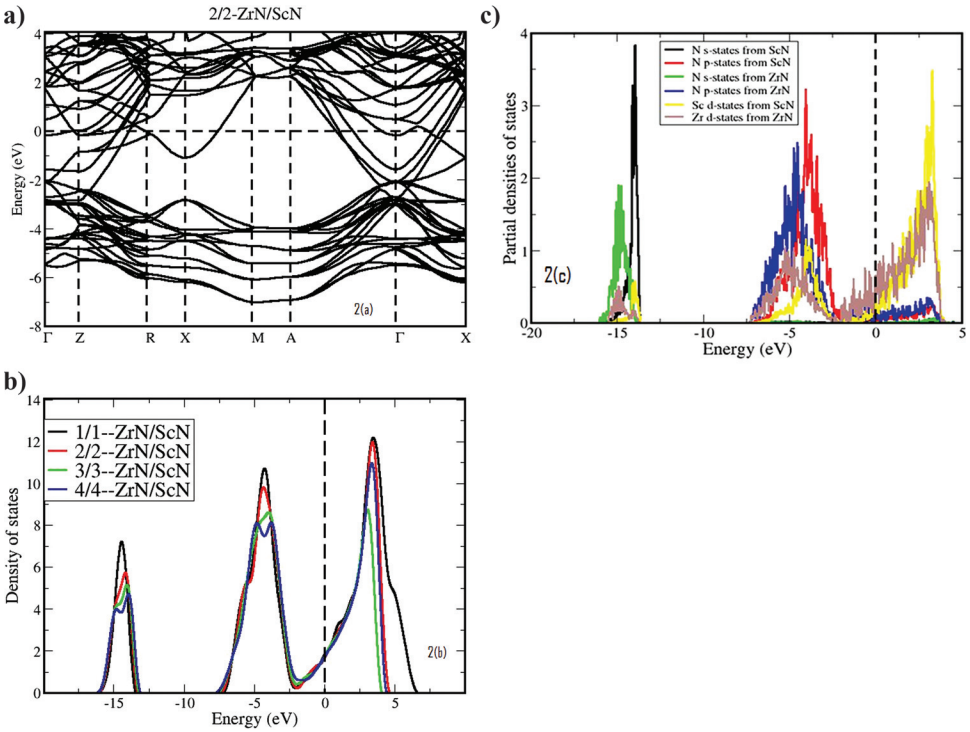

FIG. 2. (Color online) (a) Electronic structure of the 2/2-ZrN/ScN metal/semiconductor superlattice along the high symmetry directions of the tetragonal Brillouin zone. The symmetry points are Γ (0, 0, 0), *X* (0, 1/2, 0), *M* (1/2, 1/2, 0), *Z* (0, 0, 1/2), *R* (0, 1/2, 1/2), *A* (1/2, 1/2, 1/2). A relatively flat band at the Fermi energy along the Γ–*Z* directions can be observed. (b) The normalized density of states for *m*/*m* ZrN/ScN superlattices. (c) The partial densities of states (PDOS) of a typical 2/2 superlattice.

without decreasing the electrical conductivity by too much, key to enhancement of ZT.

The normalized density of states exhibits a large asymmetry at the Fermi energy [see Fig. 2(b)] (a much higher density of states at $E \geq E_F$ than at $E \leq E_F$), which is necessary within the Mahan and Sofo[24] theory for large thermopower. The partial densities of states (PDOS) [see Fig. 2(c)] indicate that the valence band nitrogen *s* and *p* states of ScN and ZrN span almost the same energy range. However, the peak positions of these nitrogen *s* and *p* states of the two nitrides are now separated by 0.88 eV and 0.65 eV, respectively. In bulk ScN and ZrN the N *s* and *p* states are separated by 2.5 eV as can be seen from our previous work.[12] Careful observation of PDOS also suggests that the peak of the Sc *d*-orbital has moved closer to the Fermi energy, with the tail of the *d*-band spanning below the Fermi energy. This shift of the Sc and N states toward the ZrN bands is significantly nonintuitive, and suggests that electronic structures of nanoscale superlattices are complicated and interesting.

To get insight into the role of electronic structure on the electrical properties of these superlattices, we have visualized [see Figs. 3(a) and 3(b)] the electronic states of the highest occupied and the lowest unoccupied states (at the Γ-point) for the 2/2-ZrN/ScN superlattice. The highest occupied electronic states (at the Γ-point) are hybridized Sc *d*-orbital and are largely confined in the ScN layers, whereas the lowest unoccupied states (at the Γ-point) are Sc and Zr *d*-states localized at the layers. This suggests that electronic states between metal and semiconductor layers at the interface are weakly coupled to each other, which will lower the electrical conductivity across the interface.

C. Estimation of Schottky barrier height

One of the most important parameters for the cross-plane electronic transport in these metal/semiconductor superlattices is the Schottky barrier height. The barrier is an intrinsic property of the interface and arises from the relative alignment between the metal Fermi level and the semiconductor valance band maximum (for *p*-type barrier) or conduction band minimum (for the *n*-type barrier) at the interface. The barrier formation mechanism and its correct estimation from the first-principles is by itself a recent field of research.[25–27] Here, we have determined the barrier height from the first-principles supercell calculations using the macroscopic averaging method.[25] The *p*-type Schottky barrier height may be written as

$$\varphi_P = E_F - E_{\mathrm{VBM}} - \Delta V,$$

where ΔV is the change in the average electrostatic potential across the interface (positive if higher on the semiconductor side), E_F is the metal Fermi level referenced to the average electrostatic potential of the bulk metal, and E_{VBM} is the valence-band maximum referenced to the average electrostatic potential of the bulk semiconductor.

Microscopic averaged electrostatic potential [shown in Fig. 4(a)] is not very smooth due to the mismatch in the lattice constants. In order to converge the band alignment, the supercell was constructed to contain eight layers of ZrN and eight layers of ScN. Table I represents our estimation of Schottky barrier height of the ZrN/ScN superlattice as a function of the periodicity of the component bulk materials. It is clear from Table I that the value of the Schottky barrier height (φ) converges as we stack 7/7 and 8/8 periods of the component materials. We do not get a reliable value of δV

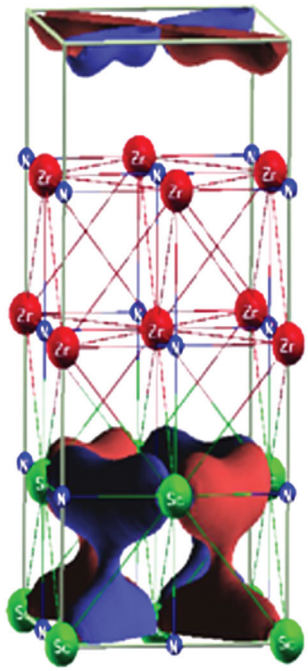

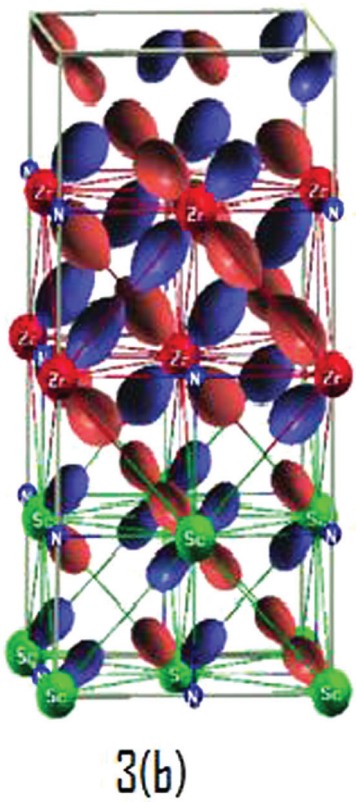

FIG. 3. (Color online) (a) Highest occupied and (b) lowest unoccupied electronic states at the Γ point for 2/2 ZrN/ScN metal/semiconductor superlattice.

when we go below the period thickness of the 6/6 superlattice, as the macroscopic averaging is not quite useful at these short length scales. Our estimates of *p*-type Schottky barrier height for the (001) interface is 0.34 eV, in reasonable agreement with the experimental value of 0.28 eV.[11] The estimated Schottky barrier height auger well with that suggested by Shakouri and co-workers[10,20,21] for filtering out the low energy electrons at the interface.

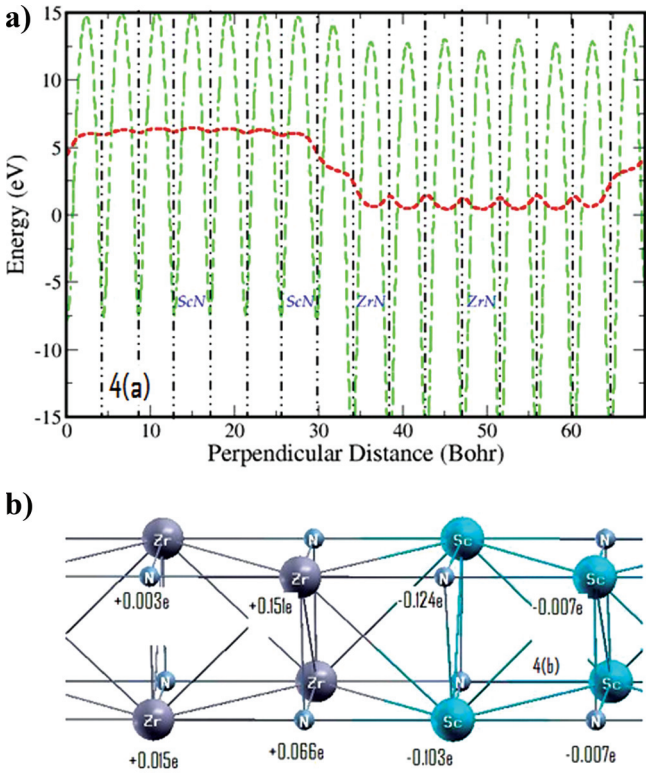

FIG. 4. (Color online) (a) Planer average electrostatic potential (oscillating dashed green line) as a function of perpendicular distance from the (001) interface. Lattice-plane oscillations are evident, and are filtered with the macroscopic averaging technique (long-dashed red line). Vertical dashed black line represents the lattice planes. The difference of microscopic average electroscopic potential between metal and semiconductor side is critical for the estimates of Schottky barrier. (b) Charge transfer from ScN to ZrN layers at the interface of 8/8 superlattices. Zr and N atoms on the ZrN layer at the interface has gained charge (indicated by the positive sign), whereas Sc and N atom on ScN layer has lost charge (shown by the negative sign), resulting in the formation of diploes.

Our calculation suggests a significant amount of charge transfer from the semiconducting (ScN) to the metallic (ZrN) layer at the interface resulting in the formation of dipoles. Figure 4(b) shows that the Sc and N atoms in the ScN layer at the interface lose equal amounts of charge to the metallic ZrN layer. Figure 4(b) also suggests that the extent of charge transferred or gained by the second layer of either the metal or the semiconductor layer from the interface is very small compared to the layers at the interface. The resulting dipole formed at the interface due to this charge transfer is

TABLE I. Estimation of Schottky barrier height as a function of the stacking period (it is clear that the value of barrier height converges with the 7/7 and 8/8 superlattices).

n/*n*-ZrN/ScN	μ_M (eV)	μ_s (eV)	δV (eV)	φ (eV)
6/6	14.54	8.81	5.306	0.42
7/7	14.54	8.81	5.411	0.33
8/8	14.54	8.81	5.392	0.34

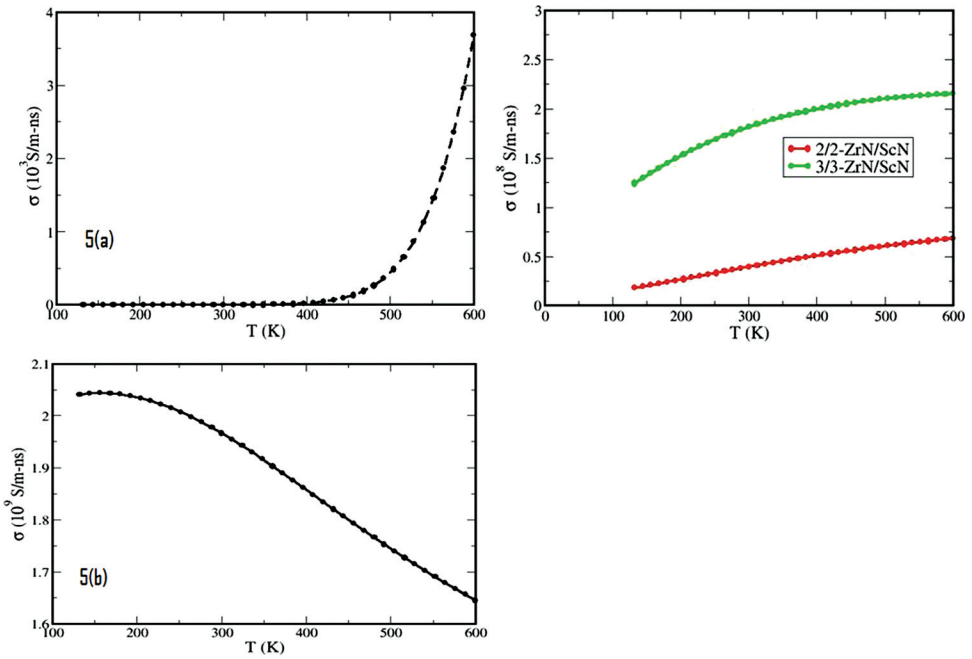

FIG. 5. (Color online) Electrical conductivity of (a) ScN, (b) ZrN, and (c) ZrN/ScN metal/semiconductor superlattices. Although the ScN and ZrN show the traditional semiconducting and metallic electrical conducting behavior, respectively, the ZrN/ScN superlattices show interesting linear increase in electrical conductivity with temperature.

accommodated for in our Schottky barrier height estimation through the macroscopic averaging method.

D. Electrical conductivity and Seebeck coefficients

Figure 5 suggests the normal Arrhenius-type temperature variation of electrical conductivity (σ) in semiconducting ScN [see Fig. 5(a)], whereas the electrical conductivity (σ) of ZrN [see Fig. 5(b)] decreases with temperature in agreement with its metallic nature. The electrical conductivity (σ) of the superlattices [see Fig. 5(c)] increases linearly with temperature, with the 3/3 superlattice having a higher σ than the 2/2 superlattice's overall temperature range. This linearly increasing behavior of σ with temperature is quite interesting as none of the conventional metals or semiconductors shows such behavior. A comparison of electrical conductivity of the superlattices with the bulk materials suggests that σ of superlattice increases by 5 orders of magnitude with respect to the semiconducting ScN; however, with respect to the metallic ZrN the electrical conductivity is one order of magnitude lower. This observation confirms our inference from band structure that these metal/semiconducting superlattices behave more like a degenerate semiconductor or semimetals having high carrier concentrations at the Fermi energy.

We have also estimated the Seebeck coefficients of superlattices and the bulk materials (ZrN and ScN). As we have taken the significant approximation of energy independent and equal relaxation time for all the materials, readers should concentrate more on the trends than the absolute values. Figure 6(a) suggests that the Seebeck coefficient (S) of the semiconductor ScN decreases with the temperature. The Seebeck coefficient of the superlattices and the metallic ZrN [see Fig. 6(b)] increases with temperature and saturates after 400 K. Figures 6(a) and 6(b) also indicate that the S of 2/2 superlattice is almost 3 times higher than the bulk ZrN, whereas S for 3/3 is closer to the metallic ZrN one. Our results also reveal an inherent trade off between electrical conductivity and Seebeck coefficient; whereas the 2/2 superlattice has lower electrical conductivity than the 3/3 one, its

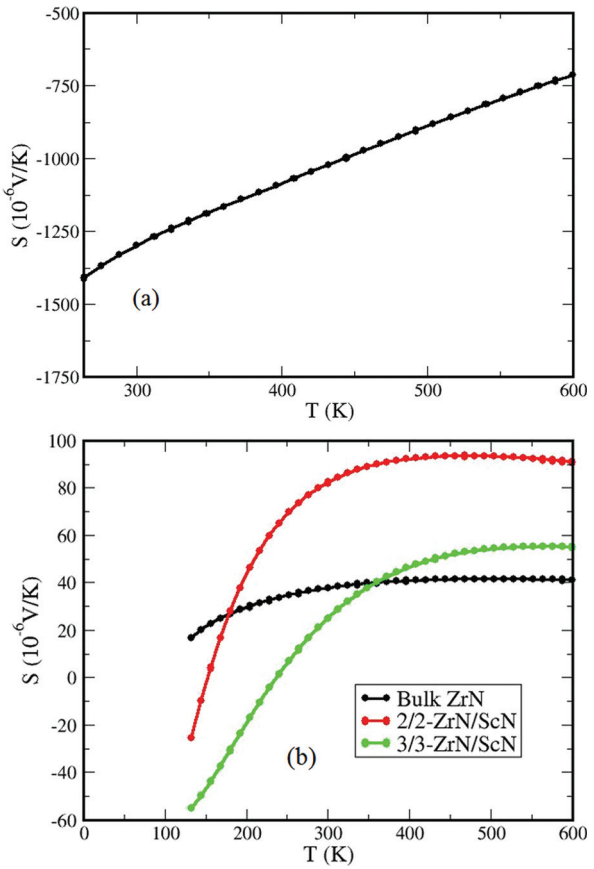

FIG. 6. (Color online) Seebeck coefficient of (a) ScN and (b) ZrN and ZrN/ScN superlattices. S of superlattices increases with temperature and saturates after 400 K.

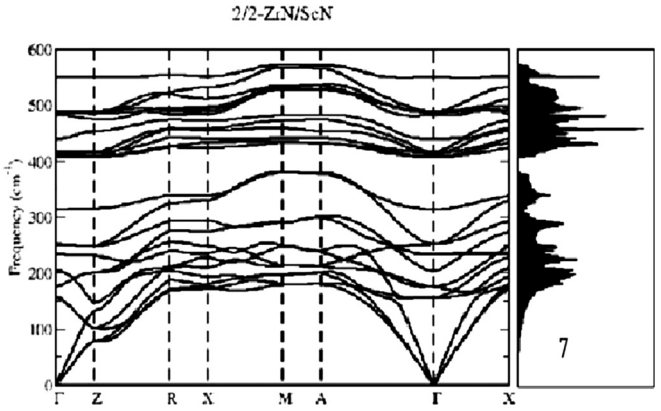

FIG. 7. Vibrational spectra and phonon density of states of 2/2 ZrN/ScN metal/semiconductor superlattices. Localized phonons, manifested as flat dispersion along the Γ–*Z*, *R*–*X*, and *M*–*A* directions are observed.

Seebeck coefficient is larger than 3/3, demonstrating that it is hard to simultaneously increase both the σ and S.

E. Vibrational spectra and thermal properties

Vibrational spectra of the 2/2 ZrN/ScN superlattices [see Fig. 7] reveal a reduction in the velocities of transverse acoustic modes along the growth direction. Due to the mismatch (large phonon densities of states of ScN in the frequency range where phonon spectrum of ZrN has a gap) in the bulk phonon density of states of the component materials,[12] the midfrequency range optical phonon bands of ScN are flattened along the cross-plane directions (i.e., Γ–*Z*, *R*–*X*, *M*–*A*) of the superlattices, making weak contributions to the lattice thermal conductivity along the cross-plane direction. On the other hand, along the in-plane directions (i.e., Γ–*X*), vibrational modes disperse as steeply as expected from the phonon dispersion of bulk materials.

We now analyze the lattice thermal conductivity using the Boltzmann transport theory. As we have not determined anharmonic interactions between phonons, it is not possible to estimate scattering times. We assume that scattering times are constant for all phonons and compare thermal conductivity of different superlattices with that of the bulk form of their components, which includes only the effects of densities of states and phonon group velocities. Our estimates of cross-plane lattice thermal conductivity [see Fig. 8(a)] κ for 1/1 superlattices are comparable to the bulk lattice thermal conductivity; whereas there is almost a tenfold reduction in κ for 2/2 superlattices compared to the 1/1 case, and to bulk ZrN. The extent of reduction is found to be even larger (almost 100 times) with respect to the bulk ScN case. This large reduction of lattice thermal conductivity can be understood in terms of the phonon filtering effect at the interface, where the mismatch in phonon density of states of the bulk materials prevents ScN mid-frequency range phonons from being propagated across the interface. This huge reduction in cross-plane lattice thermal conductivity makes these superlattices very suitable for optimizing ZT for thermoelectric energy conversion devices. Our estimates of κ are upper bound on κ as the scattering time τ is expected to be smaller for superlattices due to additional scattering at the interfaces,

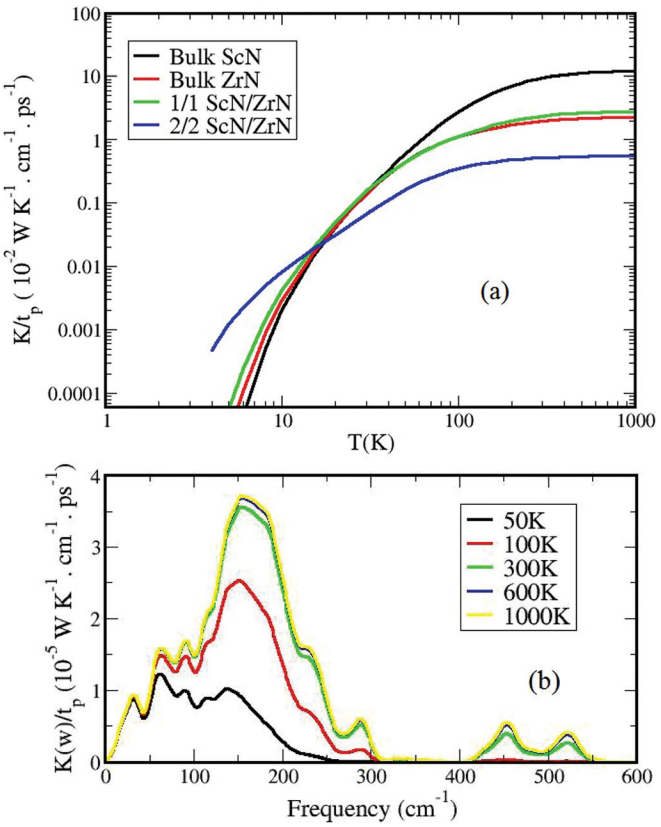

FIG. 8. (Color online) (a) Boltzmann transport based calculations of cross-plane lattice thermal conductivity for bulk materials and superlattices, representing reduction of κ along the cross-plane direction. (b) Cross-plane lattice thermal conductivity as a function of phonon frequencies at different temperatures.

reducing κ even further. Examination of the temperature variation of cross-plane lattice thermal conductivity reveals the dominance of acoustic phonons at low temperatures [see Fig. 8(b)], as temperature is increased optical phonons also start contributing to the overall lattice thermal conductivity.

IV. CONCLUSION

In summary, we have determined electronic structure, vibrational spectra, and transport properties of ZrN/ScN metal/semiconductor superlattices from first-principles calculations. Our results show the presence of asymmetry in the electronic DOS, and flattening of bands near the Fermi energy along the cross-plane direction of these superlattices. The estimated *p*-type Schottky barrier height of 0.34 eV (in good agreement with the experimental estimates) is suitable for filtering out low energy electrons at the interface of these superlattices. Electrical conductivity and Seebeck coefficient as a function of temperature of these superlattices are estimated within Boltzmann transport theory, and their values are compared. Analysis of vibrational spectra and Boltzmann transport theory-based calculations show a large reduction in lattice thermal conductivity along the cross-plane direction of these superlattices with respect to their individual bulk components as the phonons are filtered at the interfaces due to mismatches in the bulk vibrational spectra. Understanding of the metal/semiconductor superlattices and their properties

developed here should be useful in the design of nanostructured superlattices with excellent thermoelectric performance.

ACKNOWLEDGMENTS

We thank IUS-STF for supporting collaborative interaction between JNCSAR and Purdue. B.S. thanks JNCASR for a fellowship, and U.V.W. thanks funding from a DAE Outstanding Researcher Grant.

[1]A. J. Minnich, M. S. Dresselhaus, Z. F. Ren, and G. Chen, Energy Environ. Sci. **2**, 466 (2009).
[2]J. Baxter, Z. Bian, G. Chen, D. Danielson, M. S. Dresselhaus, A. G. Fedorov, T. S. Fisher, C. W. Jones, E. Maginn, U. Kortshagen, A. Manthiram, A. Nozik, D. R. Rolison, T. Sands, L. Shi, D. Sholl, and Y. Wu, Energy Environ. Sci. **2**, 559 (2009).
[3]J. Androulakis, C. H. Lin, H. J. Kong, C. Uher, C. I. Wu, T. Hogan, B. A. Cook, T. Caillat, K. M. Paraskevopoulos, and M. G. Kanatzidis, J. Am. Chem. Soc. **129**, 9780 (2007).
[4]J. P. Heremans, V. Jovovic, E. S. Toberer, A. Saramat, K. Kurosaki, A. Charoenphakdee, S. Yamanaka, and G. J. Snyder, Science **321**, 554 (2008).
[5]L. D. Hicks and M. S. Dresselhaus, Phys. Rev. B **47**, 16631 (1993).
[6]L. D. Hicks and M. S. Dresselhaus, Phys. Rev. B **47**, 12727 (1993).
[7]T. C. Harman, P. J. Taylor, M. P. Walsh, and B. E. LaForge, Science **297**, 2229 (2002).
[8]R. Venkatasubramanian, E. Siivola, T. Colpitts, and B. O'Quinn, Nature **413**, 597 (2001).
[9]A. Shakouri, in *Proceedings of International Conference on Thermoelectronics*, pp. 492–495, Clemson, SC, June 2005.
[10]D. Vashaee and A. Shakouri, Phys. Rev. Lett. **92**, 106103 (2004).
[11]M. Zebarzadi, Z. Bian, R. Singh, A. Shakouri, R. Wortman, V. Rawat, and T. D. Sands, J. Electron. Mater. **38**, 960–963 (2009).
[12]B. Saha, J. Acharya, T. D. Sands, and U. V. Waghmare, J. Appl. Phys. **107**, 033715 (2010).
[13]V. Rawat, Y. K. Kho, D. G. Cahill, and T. D. Sands, J. Appl. Phys. **105**, 024909 (2009).
[14]J. P. Perdew, K. Burke, and M. Ernzehof, Phys. Rev. Lett. **77**, 3865 (1996).
[15]D. Vanderbilt, Phys. Rev. B **41**, 7892 (1990).
[16]H. J. Monkhorst and J. D. Pack, Phys. Rev. B **13**, 5188 (1976).
[17]M. Methfessel and A. Paxton, Phys. Rev. B **40**, 3616 (1991).
[18]V. I. Anisimov and O. Gunnarson, Phys. Rev. B **43**, 7570 (1991).
[19]S. Baroni, S. D. Gironcoli, A. D. Corso, and P. Giannozzi, Rev. Mod. Phys. **73**, 515 (2000).
[20]J. M. O. Zide, D. Vashaee, Z. X. Bian, G. Zeng, J. E. Bowers, A. Shakouri, and A. C. Gossard, Phys. Rev. B **74**, 205335 (2006).
[21]D. Vashaee and A. Shakouri, J. Appl. Phys. **95**, 1233 (2004).
[22]G. D. Mahan and L. M. Woods, Phys. Rev. Lett. **80**, 4016 (1998).
[23]C. B. Vining and G. D. Mahan, J. Appl. Phys. **86**, 6852 (1999).
[24]G. D. Mahan and J. O. Sofo, Proc. Nat. Acad. Sci. U.S.A. **93**, 7436 (1996).
[25]R. T. Tung, Phys. Rev. B **64**, 205310 (2001).
[26]K. T. Delaney, N. A. Spaldin, and C. D. Van de Walle, Phys. Rev. B **81**, 165312 (2010).
[27]A. Baldereschi, S. Baroni, and R. Resta, Phys. Rev. Lett. **61**, 734 (1988).